Available online at www.sciencedirect.com
SCIENCE DIRECT®
Biomaterials 25 (2004) 3155–3161
Biomaterials
www.elsevier.com/locate/biomaterials

Structural characterization of room-temperature synthesized nano-sized β-tricalcium phosphate

Jong-Shing Bow[a], Sz-Chian Liou[b], San-Yuan Chen[b,*]

[a] QA12A/FA of United Microelectronics Cooperation, Tainan 744, Taiwan, Republic of China
[b] Department of Materials Science and Engineering, National Chiao-Tung University, 1001 Ta-hsueh Rd., Hsinchu 300, Taiwan, Republic of China

Received 2 July 2003; accepted 30 September 2003

Abstract

A simple route for synthesizing nano-sized β-tricalcium phosphate (β-TCP) at room temperature has been developed in methanol solvent. The phase evolution from $CaHPO_4$, intermediate amorphous calcium phosphate (ACP) phases (including ACP1 and ACP2 with different structures) to final β-TCP with increasing aging time was observed. The formation of β-TCP phase is favored due to the incorporation of carbonate which can suppress the transformation of ACP1 phase. High-resolution transmission electron microscopy image along [1 –1 0 0] zone axis of β-TCP reveals two types of lattice fringes (straight and wavy fringes) in β-TCP structure due to structural imperfection. Furthermore, the observations of abnormal diffraction intensity and superlattice diffraction in selected-area diffraction patterns further confirm the chemical order–disorder characteristics in β-TCP structure and can be used to elucidate the resorbability of β-TCP in either in vivo or in vitro environment due to the imperfection in β-TCP crystal.

Keywords: β-tricalcium phosphate; Electron-energy loss near-edge structure; High-resolution transmission electron microscopy; Superlattice diffraction

1. Introduction

Calcium phosphate ceramics (CPCs) have long been received a great deal of attention as a primary group of candidates for a number of biomedical applications such as orthopedics, dentistry and drug delivery, because they exhibit considerably improved biological affinity and activity, compared to currently existing synthetic materials, to surrounding host tissues when implanted. Among these CPCs, particular attention has been placed to hydroxyapatite $Ca_{10}(PO_4)_6(OH)_2$ (HA) and β-tricalcium phosphate β-$Ca_3(PO_4)_2$ (β-TCP) due to their outstanding biological responses to physiological environments [1]. Because of the chemical similarity between HA and mineralized bone of human, synthetic HA exhibits strong affinity to host hard tissues [1]. On the other hand, TCP has been proved to be resorbable in vivo with new bone growth replacing the implanted TCP [2]. This property imparts significant advantage onto TCP compared to other biomedical materials that are not resorbed and replaced by natural bone.

Conventionally, β-TCP powders are synthesized via solid-state process [3–6] and wet-chemical method [7–11]. The latter method was most commonly used to form the Ca-deficient apatite (CDHA) with the chemical formula of $Ca_9(HPO_4)(PO_4)_5(OH)$. The molar ratio of Ca/P in CDHA is the same as that in TCP, and the CDHA is usually calcined above 700–800°C to transform into β-TCP, as described by the following equation:

$$Ca_9(HPO_4)(PO_4)_5(OH) \rightarrow 3Ca_3(PO_4)_2 + H_2O. \quad (1)$$

The synthesis of β-TCP, especially at room temperature, has been very useful but never studied and reported according to our literature review work. Furthermore, it was reported that the resorbability of β-TCP in vivo might be strongly related to the characterization and stability of the β-TCP structure [12]. However, no detailed structure analysis of β-TCP phase has been systematically studied by using electron-diffraction technique and high-resolution transmission electron microscopy (HRTEM).

*Corresponding author. Tel.: +886-3-5731818; fax: +886-3-5725490.
E-mail address: sychen@cc.nctu.edu.tw (S.-Y. Chen).

0142-9612/$ - see front matter © 2003 Elsevier Ltd. All rights reserved.
doi:10.1016/j.biomaterials.2003.10.046

In this paper, the synthesis of β-TCP at room temperature in methanol will be proposed and discussed. In contrast, similar precursors and process have been prepared in the aqueous solution [7] but only CDHA instead of β-TCP phase was obtained. In addition, the electron diffraction technique, i.e. selected-area diffraction (SAD) and HRTEM will be performed to clarify the microstructure of β-TCP and to elucidate the stability and resorbability of β-TCP in either in vivo or in vitro environment.

2. Experimental procedure

2.1. Sample preparation

The preparation process was similar to our previous report [13]. The starting materials used in this investigation were analytical grade $(CH_3COO)_2Ca \cdot xH_2O$ (99%, Aldrich Chemical company, Inc., USA) as the Ca sources, and H_3PO_4 (99%, Riedel-deHaen, Seelze, Germany) as the P sources. Anhydrous methanol (99.5 wt%, GR. Merck) was used as solvent. The 0.01 mol H_3PO_4 was first dissolved in methanol. Subsequently, 0.015 mol $(CH_3COO)_2Ca \cdot xH_2O$ powder was slowly added into the same beaker at constant vigorous stirring for different aging periods of time. All the procedures were processed at room temperature ($\sim$25°C). After filtering, the white powder was finally obtained after drying overnight at 80°C.

2.2. X-ray diffractometer analysis

X-ray diffractometer (M18XHF, MAC Science, Tokyo, Japan) was used to determine the crystalline phase of the synthesized compounds at a scanning rate of 4° (2θ) per min over a 2θ range of 20–60°.

2.3. Fourier transform infrared (FT-IR) spectrometer

FT-IR spectra were performed using KBr pellets (2 mg per 300 mg KBr) on a spectrometer (Model 580, Perkin-Elmer) with a resolution of 4.00 cm^{-1}. Infrared spectra were recorded in the range of 4000–400 cm^{-1} to evaluate the function group of the specimens.

2.4. High-resolution transmission electron microscopy (HRTEM) analysis

The powder sample was ultrasonically dispersed in acetone to form very dilute suspensions and then the dilute solution was dropped on a copper grid with carbon film coated. Microstructure observation was performed with a Philips Tecnai 20 (Holland, The Netherlands) HRTEM operated at 200 kV. A double-tilt specimen holder was used to tilt several zone axes. High-resolution images were recorded at several exact zone axes with Scherzer defocus at –67 nm and at an electron-optical magnification of 490,000 to 520,000. The HRTEM was equipped with a Gatan image filter (GIF, Model 2000, Gatan) which provides chemical information with high lateral resolution and high-energy resolution. Electron energy loss spectroscopy (EELS) spectra were recorded with an energy resolution of 1.2 eV (full-width at half-maximum, FWHM, of zero-loss peak) and an energy dispersion of 0.3 eV per channel. The atomic model was established by using CaRIne crystallography software 3.1.

3. Results and discussion

3.1. Phase identification and evolution

Fig. 1 shows the X-ray diffraction (XRD) patterns of the synthetic powders in methanol with aging time from 0.5 to 8 h. In the early aging stage, the XRD pattern of the synthetic powder is identified to be $CaHPO_4$ according to ICDD No. 77–128. The diffraction peaks become broadening with increasing aging time up to 1 h. The $CaHPO_4$ phase disappeared and an amorphous calcium phosphate phase (assigned ACP1) was formed with a broad peak near $\sim$32° for 2 h-aged powder. However, the broad peak was shifted toward 31° (as calibrated by an internal standard of Si powder) with increasing aging time to 4 h. It seems to reveal that the ACP phase (assigned ACP2) aged in 4 h is not identical to the ACP1 phase (aged in 2 h). Apparently, two amorphous calcium phosphate phases, named ACP1 and ACP2, were observed in this study with aging in 2 and 4 h in the methanol, respectively. In addition, after the powder was aged in 8 h, the XRD patterns in Fig. 1 show that the crystalline β-TCP (β-$Ca_3(PO_4)_2$) phase has been formed according to ICDD No. 9-169.

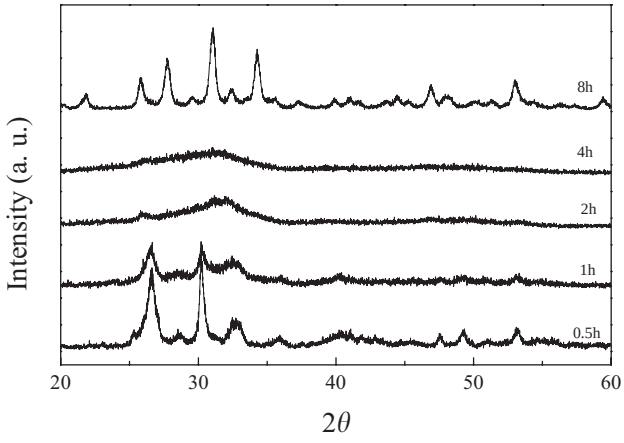

Fig. 1. X-ray diffraction (XRD) patterns of synthetic powders prepared in methanol with aging time from 0.5 to 8 h.

In order to identify the molecular arrangement of the precipitated powders, FT-IR analysis was performed. Fig. 2 illustrates the representative FT-IR spectra of the synthetic powder prepared in methanol. It clearly shows the presence of two characteristic ν_4 PO_4 bands at around 563 and 600 cm^{-1}, and ν_3 PO_4 band in the range of 1100–1000 cm^{-1} in all the cases [7]. The presence of bands at 1115, 1096, 1007 and 944 cm^{-1} can be assigned to PO_4^{3-} groups of β-TCP [13,14]. These broad and featureless PO_4^{3-} bands at 1092–1040 cm^{-1} also suggest that the resulting crystals exhibit amorphous structure, in agreement with XRD results. The splitting of the degenerate PO_4^{3-} ν_3 and ν_4 bands gradually appears in the β-TCP crystal. This observation appears to be a result of site-symmetry splitting of the degenerate modes as the environment of the PO_4^{3-} groups becomes more structurally ordered. Similar changes in FT-IR spectra were also reported in literature [14–17]. Hydroxyl groups were also discerned at 1640 and 3400 cm^{-1}. Furthermore, comparing the FT-IR spectra of ACP and β-TCP further reveals that ACP phases contain a larger amount of hydroxyl group as evidenced from the peak at 3400 cm^{-1}. It was believed that this hydroxyl group is associated with the adsorbed methanol molecules (assigned as MOH). It seems to reveal that this adsorbed hydroxyl groups, associated from the adsorbed methanol molecules, could stabilize ACP in the non-aqueous environment. Incidentally, numerous carbonate groups (CO_3^-) are also present at 875 cm^{-1} (ν_2 mode) and around 1420–1480 cm^{-1} corresponding to ν_3 mode. The formation of CO_3- is considered to be associated with the breaking of Ca–CH_3COO ionic bonds in alcohol solvents, and this process may further influence the subsequent phase transformation from ACP to another crystalline phase. Furthermore, when the synthetic powders of either $CaHPO_4$, ACP1 or ACP2 were heated above 700°C, this carbonate groups disappeared (not shown here). It seems to indicate that the carbonate groups may suppress the phase transformation process at either room temperature or high temperature.

Fig. 3(a) shows the TEM bright-field image of the synthetic CPCs powders with aging time of 3 h in methanol. It is interesting to observe two different morphologies of ACP: One is needle-like shape and the other is spherical shape. Furthermore, with increasing aging time, as shown in Fig. 1, the needle particles corresponding to ACP1 disappear but the sphere particles remain and keep growing to form ACP2.

In an attempt to further analyze the crystal structure of ACP1 and ACP2, electron energy loss spectroscopy (EELS), especially electron-energy loss near-edge structure (ELNES), is employed to explore subtle variation in the local structure of nano-scale regions such as nano-sized crystals or powders [18]. The ELNES of an

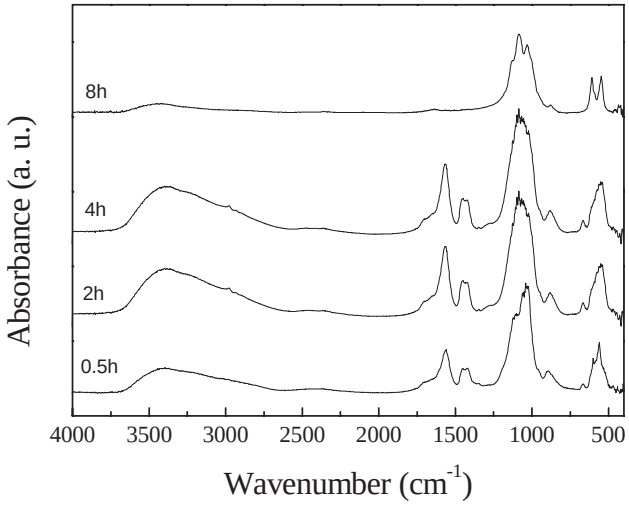

Fig. 2. Typically representative FT-IR spectra of synthetic CPCs powders prepared in methanol.

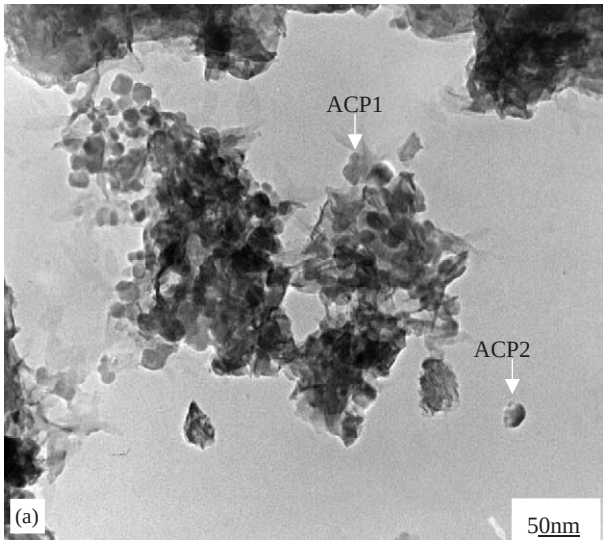

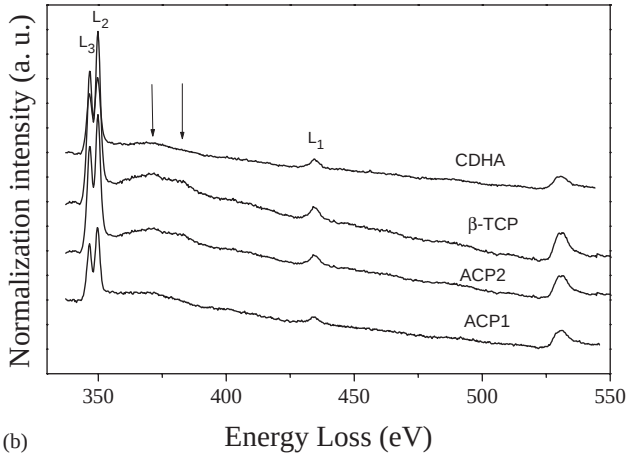

Fig. 3. (a) Transmission electron microscopy (TEM) bright-field (BF) image of synthetic CPCs powders aged in methanol for 3 h and (b) ELNES spectra of Ca$L_{2,3}$-edge and L_1-edge for synthetic CPCs powders with different phases.

element can be the fingerprint of its chemical bonding state and can be compared to study the crystallographic relationship between the synthetic CPCs powders.

After background subtraction, the ELNES of Ca $L_{2,3}$-edge and L_1-edge for the synthetic CPCs powders are shown in Fig. 3(b). Following the dipole selection rule, the L_3 and L_2 edge spectra are transitions of $2p^{3/2} \rightarrow 3d^{3/2}3d^{5/2}$ and $2p^{1/2} \rightarrow 3d^{3/2}$, respectively [18,19]. The L_1-edge appearing in the EELS spectrum indicates that the 4p orbitals are not filled in the synthetic CPCs powders. It was observed that the ELNES feature of ACP2 is similar to that of β-TCP, indicating that the coordination of Ca atoms is similar between these two phases. This result is consistent with the work of the extended X-ray absorption fine structure (EXAFS) reported by Liou et al. [13] and Harris [20]. It was reported that the transformation of ACP into crystalline β-TCP proceeds without any change in the local environment of Ca but with the development of long-range order and the removal of certain amount of water. The fine structure of ELNES spectra in Fig. 3(b) further reveals that the ELNES of ACP1 is very similar to that of Ca-deficient apatite (CDHA) prepared in aqueous solution with Ca/P ratio of 1.5 [7,19]. It implies that both ACP1 and CDHA have the same bonding state and site symmetry around Ca atoms. According to the reported literature, the structure of ACP presents the form of either $Ca_9(PO_4)_6 \cdot EtOH$ [16] or $Ca_3(PO_4)_2 \cdot H_2O$ [13]. Therefore, it may be suggested that the ACP1 is HA-like structure with chemical formula of $Ca_9(PO_4)_6 \cdot MOH$, where M is CH_3 and ACP2 is β-TCP-like structure with chemical formula of $Ca_3(PO_4)_2 \cdot MOH$ [13].

The phase evolution with aging time in methanol can be further interpreted as follows. After the H_3PO_4 was added in methanol solvent, a clear solution was observed. However, colloidal particles were visually detected in the solutions after adding the Ca precursor into these H_3PO_4-methanol solution. It seem to imply that the addition of Ca precursor results in the inter-reaction of Ca with P ions to form Ca-P compounds through the following reaction:

$$Ca^{2+} H_3PO_4 \rightarrow CaHPO_4 + \text{amorphous Ca-P complex.} \quad (2)$$

A further reaction in Eq. (2) leads to the formation of an amorphous calcium phosphate ACP1 with the diffraction peaked at $2\theta \approx 32^\circ$;

$$CaHPO_4 + \text{amorphous Ca-P complex} \rightarrow \text{ACP1.} \quad (3)$$

According to the reported literature [21,22], the metastable ACP phase having HA-like structure can be only converted into stable crystalline HA by a process of dissolution and renucleation in water slurries and under specific chemical conditions (i.e. high temperature, low super-saturation and ionic strength, and neutral pH). Therefore, with the incorporation of carbonate, dissociated from calcium acetate, the transformation of ACP1 with HA-like structure into poorly crystalline CDHA phase will be suppressed in this study. On the other hand, the ACP1 would be converted into ACP2 along with morphology changing from needle to sphere. As evidenced from XRD patterns, the diffraction peak near 31° (for ACP2) instead of 32° (for ACP1) was developed.

The ACP2 structure was identified to be β-TCP-like structure according to our previous study by using EELS and EXAFS [13]. In addition, since both ACP2 and β-TCP have similar structure, a further removal of the carbonate and hydroxyl groups from ACP2 is favorable to built long-range order of crystalline β-TCP without experiencing structural change as follows:

$$\text{ACP2} \rightarrow \beta\text{-}Ca_3(PO_4)_2 \text{ (crystalline).} \quad (4)$$

3.2. Structural analysis of β-TCP

The TEM micrographs of β-TCP phase formed in methanol are shown in Fig. 4(a). It clearly reveals that

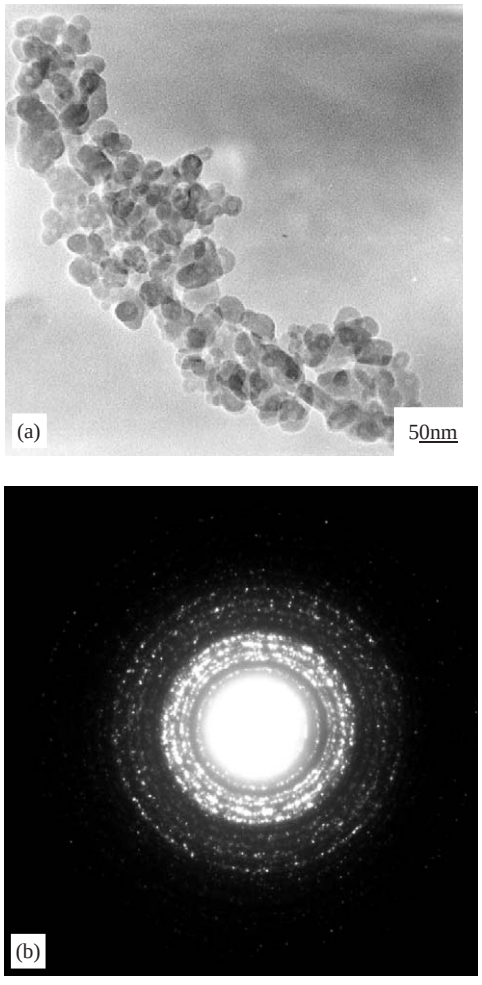

Fig. 4. (a) TEM micrographs of β-TCP phase obtained in pure methanol and (b) corresponding selected area diffraction pattern (SADP) of (a).

the dimension of the spherical β-TCP crystal is around 50 nm in diameter. The electron diffraction techniques such as selected-area diffraction (SAD) take several advantages over X-ray and neutron powder diffraction approaches, i.e., the tunable spot size of electron beam and the high sensitivity of electrons to the electrostatic potential of studied samples [23]. As shown in Fig. 4(b), the ring patterns of the β-TCP crystals display all the possible reflections of β-TCP crystals but those rings corresponding to the first three values of d-spacings are not shown in this figure due to the high intensity of the transmitted beam. A set of d-spacing values of crystal planes of β-TCP is given in Table 1. The ring formed by diffraction spots of a specific $\{h\ k\ l\}$ crystal planes is not a sharp circle but has a certain width. This broadening may be caused by imperfection in crystallization as well as nano-size effect. These two factors cannot be identified by neither electron diffraction technique or XRD. Therefore, HRTEM was used to study the structural characteristics and would be discussed later.

Fig. 5(a) shows a selected-area diffraction pattern (SADP) along the zone axis [1 –1 0 0] of β-TCP. The miller index of diffraction spot reflecting the diffraction plane in real space was calculated in Fig. 5(b). It clearly reveals that there exists a set of weak extra diffraction spots located at halfway between the central (0 0 0) spot and the {0 0 0 6} spots and are indexed as {0 0 0 3} superlattice diffraction spots. These extra spots could be caused by chemical order or double diffraction along this zone axis. If double diffraction occurs in this study, it is possible to view Moiré fringes somewhere in the corresponding TEM image. However, no Moiré fringes were observed, indicating that the effect of chemical order is primarily associated with these superlattice reflections.

Table 1
d-spacing measurement and corresponding possible crystal planes ($h\,k\,l$) of β-TCP

Ring	Measuring distance (cm)	d-spacing (Å)	Corresponding ($h\,k\,l$)
1	3.100	8.097	(0 1 2)
2	3.880	6.469	(1 0 4)
3	4.800	5.229	(1 1 0)
4	5.175	4.850	(1 1 3)
5	7.300	3.438	(1 0 10)
6	7.775	3.228	(2 1 4)
7	8.275	3.033	(3 0 0)
8	8.700	2.885	(0 2 10)
9	9.050	2.773	(1 2 8)
10	9.550	2.628	(2 2 0)
11	9.875	2.542	(2 1 10)
12	10.600	2.368	(3 1 5)

$\lambda L = Rd$ where λ is the electron wavelength of using TEM machine ($\lambda = 0.00251$ nm in this study), L ceramic length (100 cm in this study), R interval between the origin and a diffraction spot or ring in a diffraction pattern and d the lattice-spacing.

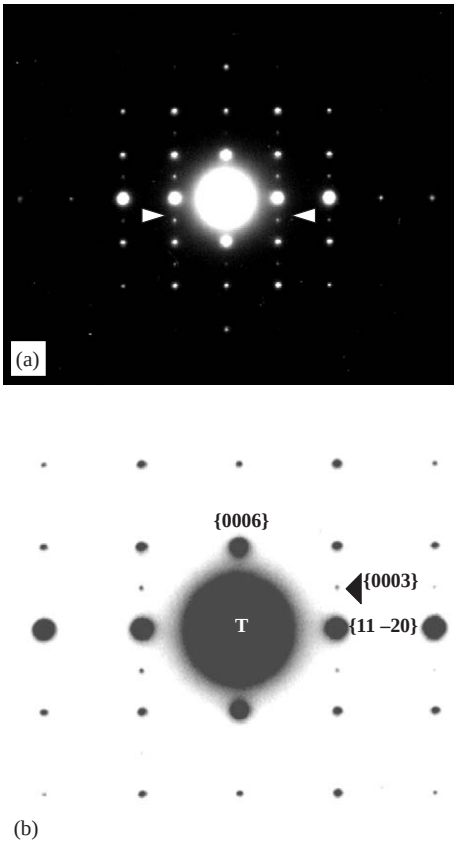

Fig. 5. (a) Selected-area diffraction pattern (SADP) and (b) corresponding diffraction plane along the zone axis [1 –1 0 0] of β-TCP.

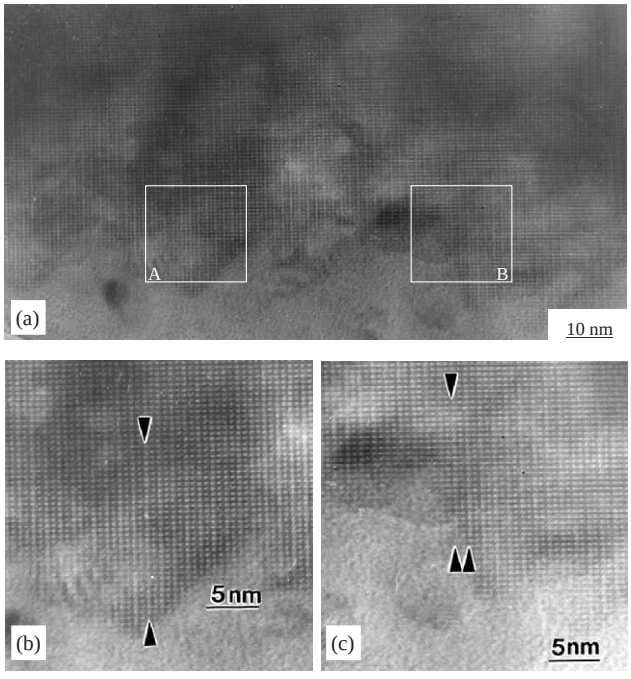

Fig. 6. (a) The lattice fringe changes with crystal tilted for several mrads from left region marked with A to right region marked with B across the picture along [1 –1 0 0] zone axis. Both regions of marked A and B were magnified in (b) and (c), respectively.

When the crystal was tilted along this [1 –1 0 0] zone axis for several mrad (less than 3 mrad) from left marked with A to right marked with B across the picture, the lattice fringe change in the HRTEM image of Fig. 6(a) is clearly observed. The regions of marked A and B were further magnified and shown in Fig. 6(b) and (c), respectively. The size and contrast of fringes between Fig. 6(b) and (c) look different as viewed from top or bottom at a glace angle. The one in Fig. 6(b) shows straight fringes but the other one in Fig. 6(c) displays alternative contrast variation with wave-like fringes. This indicates that the analyzed β-TCP crystal is not a perfect single crystal. This variation in the lattice fringes as marked with arrows results from two types of crystal arrangements due to the induced extra diffraction spot in SADP.

Based on the refinement result of β-TCP reported by Dickens et al. [24], the structural model of β-TCP along [1 –1 0] zone axis can be schematically illustrated in Fig. 7 by using CaRIne software and the structural simulation can be further confirmed by HRTEM images. It implies that there are two types of Ca-PO_4 chains: one is straight chain and the other is wavy chain as indicated with square A and B in Fig. 7, respectively. If this β-TCP structural model is right, two arrangements should coexist along this [1 –1 0] zone axis in β-TCP structure. As viewed along the [1 –1 0 0] zone axis, two HRTEM images were taken and shown in Fig. 8(a) and (b), respectively. Two types of lattice fringes can be clearly identified: one with straight fringes (Fig. 8(a)), corresponding to the square A in Fig. 7, and the other with stepper chains or wave-like fringes (Fig. 8(b)), corresponding to the square B in Fig. 7. It may be considered that the wave-like fringes result from an imperfect crystal where the long-range order has not been completely constructed. So far, to authors' knowledge, this phenomenon has never been reported in the literature. However, it is believed that the structural imperfection in the B-TCP crystal as demonstrated in this study by HRTEM observation often offers sites for resorption and this could be used to elucidate the resorbility of β-TCP in either in vivo or in vitro environment.

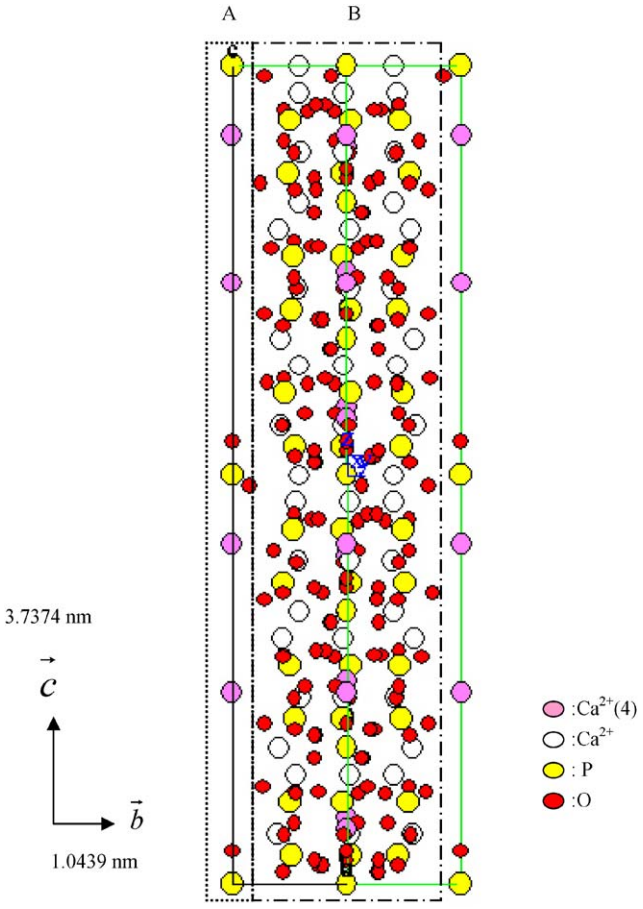

Fig. 7. Schematically structural model of β-TCP along [1 –1 0] zone axis. Marked square A: straight array of Ca-PO_4 chain and B: stepper or wave-like of Ca-PO_4 chain.

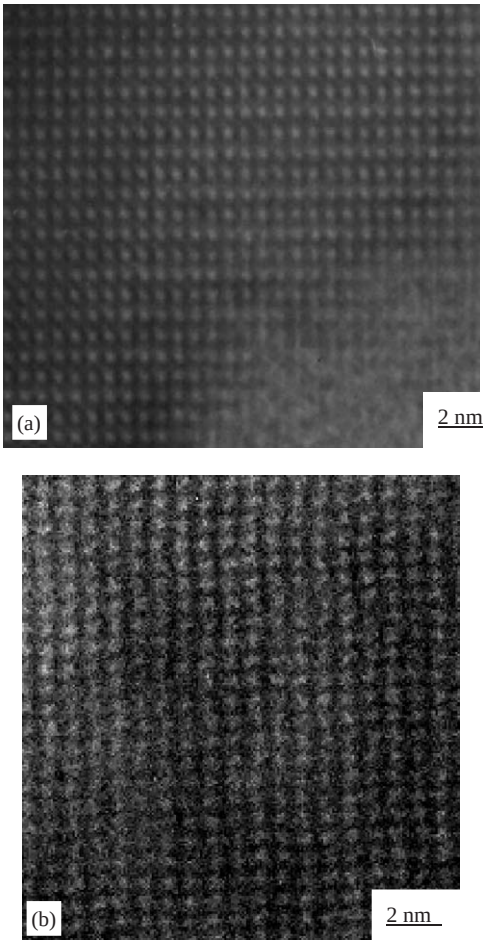

Fig. 8. Two types of HRTEM lattice fringes were observed as viewed along the [1 –1 0 0] zone axis: (a) straight fringes and (b) stepper chains or wave-like fringes.

4. Conclusions

Nano-sized β-TCP phase with $\sim$50 nm in diameter can be well synthesized at room temperature. The incorporation of carbonate plays an important role in suppressing the transformation of ACP1 phase with HA-like structure into poorly crystalline CDHA but favoring the formation of β-TCP phase. The observations of abnormal diffraction intensity and superlattice diffraction in SADP strongly provide the chemical order information in β-TCP structure. High-resolution TEM image along [1 –1 0 0] zone axis of β-TCP reveals two types of lattice fringes (straight and wavy fringes) in β-TCP structure due to structural imperfection that could be used to elucidate the resorbability of β-TCP in either in vivo or in vitro environment.

Acknowledgements

The authors gratefully acknowledge the National Science Council of the Republic of China for its financial support through Contract No. NSC-92-2216-E-009-025.

References

[1] Kivrak N, Tas AC. Synthesis of calcium hydroxyapatite-tricalcium phosphate (HA-TCP) composite bioceramics powders and their sintering behavior. J Am Ceram Soc 1998;81(9): 2245–52.
[2] Gibson IR, Rehman I, Best SM, Bonfield W. Characterization of the transformation from calcium-deficient apatite to β-tricalcium phosphate. J Mater Sci.: Mater Med 2000;12:799–804.
[3] Bigi A, Foresti E, Gandolfi M, Gazzano M, Roveri N. Isomorphous substitutions in β-tricalcium phosphate: the different effects of zinc and strontium. J Inorg Biochem 1997;66: 259–65.
[4] Yokogawa Y, Kawamoto Y, Toriyama M, Suzuki T, Kawamura S. Tricalcium phosphate coating on zirconia using calcium metaphosphate and tetracalcium phosphate. J Ceram Soc Jpn 1991;99:28–31.
[5] Famery R, Richard N, Boch P. Preparation of α- and β-tricalcium phosphate ceramics, with and without magnesium addition. Ceram Int 1994;20:327–36.
[6] Pan Y, Huang JL, Shao CY. Preparation of β-TCP with high thermal stability by solid reaction routs. J Mater Sci 2003;38:1049–56.
[7] Liou SC, Chen SY. Transformation mechanism of different chemically precipitated apatitic precursors into β-tricalcium phosphate upon calcinations. Biomaterials 2002;23:4541–7.
[8] Jarcho M, Salsbury RL, Thomas MB, Doremus RH. Synthesis and fabrication of β-tricalcium phosphate (whitlockite) ceramics for potential prosthetic applications. J Mater Sci 1979;14:142–50.
[9] Akao M, Aoki H, Kato K, Sato A. Dence Polycrystalline β-tricalcium phosphate for prosthetic applications. J Mater Sci 1982;17:343–6.
[10] Itatani K, Nishioka T, Seike S, Howell FS, Kishioka A, Kinoshita M. Sinterability of β-calcium orthophosphate powder prepared by spray-pyrolysis. J Am Ceram Soc 1994;77(3):801–5.
[11] Tas AC, Korkusus F, Timucin M, Akkas N. An investigation of the chemical synthesis and high-temperature sintering behavior of calcium hydroxyapatite (HA) and tricalcium phosphate (TCP) bioceramics. J Mater Sci Mater Med 1997;8:91–6.
[12] Okazaki M, Sato M. Computer graphics of hydroxyapatite and β-tricalcium phosphate. Biomaterials 1990;11:573–8.
[13] Liou SC, Chen SY, Liu DM. Manipulation of phase development and structural characterization of calcium phosphate ceramics-polymer nanocomposites at ambient temperature in water-methanol mixtures. J Mater Sci Mater Med, submitted for publication.
[14] Vallet-Regi M, Rodriguez-Lorenzo LM, Salinas AJ. Synthesis and characterization of calcium deficient apatite. Solid State Ionic 1997;101–103:1279–85.
[15] Layrolle P, Lebugle A. Characterization and reactivity of nanosized calcium phosphates prepared in anhydrous ethanol. Chem Mater 1994;6:1996–2004.
[16] Lerner E, Azoury R, Sarig S. Rapid precipitation of apatite from ethanol-water solution. J Crystal Growth 1989;97:725–30.
[17] Liu DM, Yang Q, Troczynski T. Sol–gel hydroxyapatite coatings on stainless steel substrates. Biomaterials 2002;23:691–8.
[18] Egerton RF. Electron energy-loss spectroscopy in the electron microscope. New York: Plenum Press; 1996.
[19] Liou SC, Chen SY, Lee HY, Bow JS. Structural characterization of nano-sized calcium deficient apatite powders. Biomaterials 2004;25:189–96.
[20] Harries JE, Hukins DWL. Conversion of amorphous calcium phosphate into hydroxyapatite investigated by EXAFS spectroscopy. J Crystal Growth 1987;84:563–70.
[21] Nancollas A. Nucleation and growth of phosphate minerals. In: Nriagu JO, Moore PB, editors. Phosphate minerals. Berlin/Heidelberg: Springer; 1984. p. 137–54.
[22] Abbona F, Franchini-Angela M. Crystallization of calcium and magnesium phosphates from solutions of low concentration. J Crystal Growth 1990;104:661–7.
[23] Williams DB, Carter CB. Transmission electron microscopy: a textbook for materials science. New York: Plenum Press; 1996. p. 478.
[24] Dickens B, Schroeder LW, Brown WE. Crystallographic studies of the role of Mg as a stabilizing impurity in β-$Ca_3(PO_4)_2$: I. The crystal structure of pure β-$Ca_3(PO_4)_2$. J Solid State Chem 1974;10:232–48.